Enhancing 5G-based Localization in Dynamic Environments through Network Digital Twins

Zhengchen Xu*, Silvia Mura*, Francesco Linsalata*,
Lorenzo Cazzella*, Damiano Badini†, and Umberto Spagnolini*
*DEIB, Politecnico di Milano, Milan, Italy *name.surname@polimi.it*
†Huawei Italy Research Center *name.surname@huawei.com*

GLOBECOM 2025 - 2025 IEEE Global Communications Conference | 979-8-3315-7781-0/25/$31.00 ©2025 IEEE | DOI: 10.1109/GLOBECOM59602.2025.11431735

***Abstract*—The increasing demand for reliable Vehicle-to-Everything (V2X) communications and autonomous mobility necessitates sophisticated simulation frameworks and intelligent optimization strategies. This paper presents a Network Digital Twin (NDT) that integrates high-fidelity ray-tracing with real vehicular traffic data to model wireless propagation in dynamic urban environments and derive theoretical localization bounds. By explicitly exploiting multipath reflections, both line-of-sight (LOS) and non-line-of-sight (NLOS), from static and mobile reflectors such as vehicles, the framework supports the design of an optimized precoding scheme for enhanced user equipment (UE) positioning. Numerical results indicate that the proposed NDT-guided method reduces the Position Error Bound (PEB) by approximately 35%, underscoring NDT benefits and the utility of NLOS exploitation for high-accuracy localization in dense urban scenarios.**

***Index Terms*—V2X, Network Digital Twin (NDT), localization**

I. Introduction

The evolution of fifth-generation (5G) networks is poised to transform intelligent transportation systems by enabling ultra-reliable, low-latency Vehicle-to-Everything (V2X) communications, a fundamental requirement for autonomous vehicle deployment [1]. Nonetheless, the dynamic and heterogeneous nature of vehicular environments presents persistent challenges for mobility-aware network management, accurate localization, and wireless channel optimization. To address these issues, the Digital Twin (DT) paradigm has emerged as a key enabler for future V2X systems, offering real-time virtual representations of physical environments to support simulation, optimization, and informed decision-making [2].

A Network Digital Twin (NDT), in particular, provides a high-fidelity wireless propagation model, capturing the spatiotemporal dynamics of vehicles, infrastructure, and communication nodes [3]. By incorporating detailed 3D maps, vehicular traffic simulations, and ray tracing techniques, the NDT enables accurate modeling of urban environments. Ray tracing enhances channel representation by characterizing multipath propagation and delivering precise channel state information, essential for beamforming and blockage mitigation [4]. Simultaneously, traffic simulations inform mobility trends, congestion patterns, and route dynamics, allowing the NDT to anticipate network conditions and support proactive strategies such as beam switching and relay selection [5].

Localization accuracy in V2X networks is often hindered by difficulties in accurately estimating channel parameters such as angle of arrival (AOA), angle of departure (AOD), and time of arrival (TOA), particularly at higher frequencies where severe path loss and signal attenuation reduce the reliability of multipath component extraction [6]. Operating at 7 GHz, an upper sub-6 GHz band, offers a favorable compromise: it provides sufficient bandwidth to support high-throughput services while mitigating the propagation challenges typical of millimeter-wave (mmWave) frequencies [7]. This intermediate frequency range allows for a more robust estimation of channel parameters in urban environments, where non-line-of-sight (NLOS) conditions dominate and high-frequency signal degradation can critically affect localization performance.

Recent localization methods leveraging Digital Twin (DT) frameworks, such as RSSI fingerprinting [8], attempt to compensate for these challenges by matching real-time signal measurements with precomputed databases. However, their performance remains limited in complex environments due to multipath interference and low spatial resolution. Traditional techniques based on TOA, TDOA, AOA, or AOD often assume the presence of a strong line-of-sight (LOS) path [9], an assumption that fails in dense urban scenarios. Hybrid approaches, including joint AOA-TOA schemes [10], offer improved resilience to NLOS conditions, but still depend heavily on accurate channel estimates and the distinguishability of multipath components.

These challenges highlight the need for localization frameworks that effectively integrate LOS and NLOS information, particularly in vehicular networks. Recent studies show that NLOS components can enhance localization accuracy by providing additional propagation paths, especially when reflectors are positioned near the transmitter (TX) or receiver (RX) [11]. However, existing research largely focuses on static reflectors, neglecting the dynamic multipath contributions from moving vehicles. Although dense vehicular deployments have been identified as a potential source of improved multipath diversity [12], the systematic integration of vehicle-induced NLOS components into localization frameworks remains underexplored.

In this context, the high-fidelity virtual environments provided by NDTs offer significant potential for adaptive localization in V2X networks. By utilizing a priori vehicular traffic data and maps, NDTs supply dynamic environmental information essential for improving localization accuracy. This paper derives theoretical positioning bounds in urban environments,

leveraging traffic and mobility data from NDTs. This approach enables the establishment of traffic-aware localization limits and allows for a systematic exploration of the role of vehicle-induced reflections in enhancing localization performance in V2X networks.

Paper Contributions The main contributions of this paper are summarized below:

- Derive a theoretical bound on position error for uplink communication by leveraging NDT to extract precise channel parameters and build accurate channel models via ray-tracing simulations.
- Exploit NDT-enabled vehicle traffic data to empirically estimate the probability of vehicle presence across the environment, allowing for realistic modeling of dynamic obstacles in urban scenarios.
- Based on the vehicle presence probabilities, we determine the likelihood that vehicles act as reflectors. We then analyze how the resulting multipath components can enhance localization accuracy, providing a more realistic and practical assessment of urban V2X communication performance.

Paper Organization The remainder of the paper is organized as follows. Section II presents the system model and the channel parameters extracted from the NDT. Section III derives the 3D localization error bound. Section IV details the traffic-aware enhancement method and the optimized beamforming scheme. Section V reports numerical results, and Section VI concludes the paper with directions for future research.

Notation Scalars are in italic (e.g., x); vectors in bold lowercase (e.g., $\mathbf{x}$); matrices in bold uppercase (e.g., $\mathbf{X}$). Matrix elements are $[\mathbf{X}]_{i,j}$, with i as the row and j the column index. Transpose and conjugate transpose are denoted by $\mathbf{X}^{\mathrm{T}}$ and $\mathbf{X}^{\mathrm{H}}$, respectively. The trace is $\mathrm{tr}(\mathbf{X})$; Euclidean norm is $||\cdot||$ (e.g., $||\mathbf{x}||$); element-wise (Hadamard) product is $\circ$.

II. System Model

We consider the uplink transmission scenario shown in Fig. 2, where the user equipment (UE), hereafter also referred to as the transmitter (TX), is located at position $\mathbf{p} = [p_x, p_y, p_z]^{\mathrm{T}}$ in a global Cartesian coordinate system with axes x, y, and z. The TX communicates with a base station (BS), acting as the receiver (RX), located at $\mathbf{b} = [b_x, b_y, b_z]^{\mathrm{T}}$. The BS aims to estimate the unknown UE position by exploiting NDT and the uplink signal.

Both the UE and BS are equipped with uniform planar arrays (UPAs), composed of N_{TX} and N_{RX} isotropic antenna elements, respectively. The antenna elements are spaced by d_h and d_v along the horizontal and vertical dimensions, respectively, with identical spacing at both the UE and BS.

The transmitted OFDM signal is given by

$$\mathbf{x}(t) \triangleq \sqrt{E_s}\mathbf{F}\mathbf{s}(t), \tag{1}$$

where E_s denotes the transmitted energy per symbol duration, and $\mathbf{F} \triangleq [\mathbf{f}_1, \mathbf{f}_2, \ldots, \mathbf{f}_{N_B}] \in \mathbb{C}^{N_{\mathrm{TX}} \times N_B}$ is the precoding matrix corresponding to N_B transmitted beams. Each precoding vector $\mathbf{f}_l(\theta_l, \phi_l)$ is defined as

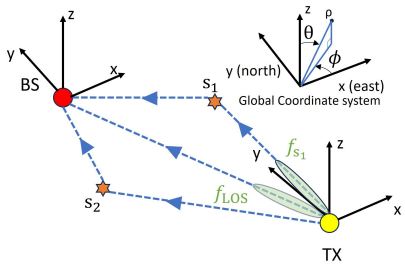

Fig. 1: Uplink transmission scenario in 3D space, where the TX communicates with the BS via multiple paths. The optimized precoder steers beams toward the LOS (f_{LOS}) and dominant NLOS (f_{s_1}) directions.

$$\mathbf{f}_l(\theta_l, \phi_l) \triangleq \frac{1}{\sqrt{N_B}}\mathbf{a}_{\mathrm{TX},l}, \tag{2}$$

where the array response is

$$\mathbf{a}_{\mathrm{TX,l}} = \frac{1}{\sqrt{N_{\mathrm{TX}}}} e^{-j\boldsymbol{\Delta}_{\mathrm{TX}}^{\mathrm{T}}\mathbf{k}(\theta_l,\phi_l)}, \tag{3}$$

with $\boldsymbol{\Delta}_{\mathrm{TX}} \in \mathbb{R}^{3\times N_{\mathrm{TX}}}$ denoting the matrix containing the TX antenna coordinates. The wave vector $\mathbf{k}(\theta,\phi) \in \mathbb{R}^{3\times 1}$ is defined as $\mathbf{k}(\theta_l,\phi_l) = \frac{2\pi}{\lambda}\left[\cos(\phi_l)\sin(\theta_l)\ \sin(\phi_l)\sin(\theta_l)\ \cos(\theta_l)\right]$, where λ is the carrier wavelength. The angles θ_l and ϕ_l represent the azimuth and elevation precoding angles, respectively, selected from a uniformly spaced beam codebook covering the angular domain.

The pilot signal is represented by $\mathbf{s}(t) = [s_1(t), \ldots, s_{N_B}(t)]^{\mathrm{T}} \in \mathbb{C}^{N_B\times 1}$, with each component given by

$$s_l(t) \triangleq \sum_{m=0}^{N_s-1} d_{l,m}\, p(t - mT_s), \tag{4}$$

where N_s is the number of pilot symbols per beam, T_s is the symbol duration, $d_{l,m}$ denotes the m^{th} unit-energy pilot symbol for the l^{th} beam, and $p(t)$ is a unit-energy pulse with associated power spectral density (PSD) $|P(f)|^2$. The transmitted power is normalized by setting $\mathrm{tr}(\mathbf{F}^{\mathrm{H}}\mathbf{F}) = 1$ and $\mathbb{E}\{\mathbf{s}(t)\mathbf{s}^{\mathrm{H}}(t)\} = \mathbf{I}_{N_B}$, where $\mathrm{tr}(\cdot)$ denotes the trace operator and $\mathbf{I}_{N_B}$ is the N_B-dimensional identity matrix.

The communication channel for the k-th path is modeled as $\mathbf{H}_k \in \mathbb{C}^{N_{\mathrm{RX}}\times N_{\mathrm{TX}}}$

$$\mathbf{H}_k = \sqrt{N_{\mathrm{TX}}N_{\mathrm{RX}}}\beta_k\, \mathbf{a}_{\mathrm{RX,k}}\, \mathbf{a}_{\mathrm{TX,k}}^{\mathrm{H}}, \tag{5}$$

where β_k is the complex channel gain for the k^{th} path, and $\mathbf{a}_{\mathrm{TX,k}}$ and $\mathbf{a}_{\mathrm{RX,k}}$ are the TX and RX steering vectors, respectively, constructed according to (3) using the associated AOD and AOA. Specifically, the azimuth and elevation AOD at the TX are denoted by $\phi_{\mathrm{TX,k}}$ and $\theta_{\mathrm{TX,k}}$, while the azimuth and elevation AOA at the RX are denoted by $\phi_{\mathrm{RX,k}}$ and $\theta_{\mathrm{RX,k}}$. The path with $k = 1$ corresponds to the LOS component, while

paths with $k \geq 2$ correspond to NLOS components. [1] We refer to the position of the kth reflector as $\mathbf{s}_k = [s_{kx}, s_{ky}, s_{kz}]^{\mathrm{T}}$.

The received signal at the RX is given by $\mathbf{r}(t) \in \mathbb{C}^{N_{\mathrm{RX}} \times N_s}$:

$$\mathbf{r}(t) = \underbrace{\sum_{k=1}^{K} \mathbf{H}_k \mathbf{x}(t - \tau_k)}_{\boldsymbol{\mu}(t)} + \mathbf{w}(t), \tag{6}$$

where $\mathbf{w}(t) \in \mathbb{C}^{N_{\mathrm{RX}} \times 1}$ denotes the additive white Gaussian noise vector with PSD N_0. Consistent with [11], it is assumed that each RX antenna is connected to a low-noise amplifier and a passband filter [2].

III. Localization Metrics and Bounds

This section introduces the performance metrics and theoretical limits relevant to 3D localization, with particular emphasis on the position error bound (PEB). The objective is to quantify the achievable localization accuracy, which can subsequently be exploited as a priori information in scenarios where NDT is employed. To this end, we begin by deriving the Fisher Information Matrix (FIM) corresponding to each individual propagation path. These derivations enable the formulation of closed-form expressions for the Cramér-Rao Lower Bound (CRLB), which serves as a benchmark for the best possible estimation accuracy and is subsequently used to compute the PEB. The communication parameters to be estimated include

$$\boldsymbol{\eta} = [\boldsymbol{\theta}_{\mathrm{RX}}, \boldsymbol{\theta}_{\mathrm{TX}}, \boldsymbol{\phi}_{\mathrm{RX}}, \boldsymbol{\phi}_{\mathrm{TX}}, \boldsymbol{\beta}_{\mathrm{R}}, \boldsymbol{\beta}_{\mathrm{I}}, \boldsymbol{\tau}], \tag{7}$$

including the azimuth and elevation AOA and AOD for each propagation path k, i.e. $\theta_{\mathrm{RX},k}$, $\phi_{\mathrm{RX},k}$, $\theta_{\mathrm{TX},k}$, and $\phi_{\mathrm{TX},k}$, as well as the real and imaginary components of the complex path gains and the corresponding propagation delays τ_k. These parameters are structured into vector form similarly to $\boldsymbol{\theta}_{\mathrm{RX}} = [\theta_{\mathrm{RX},1}, \ldots, \theta_{\mathrm{RX},K}]^{\mathrm{T}} \in \mathbb{R}^{K \times 1}$.

The Fisher Information Matrix (FIM), denoted by $\mathbf{J}(\boldsymbol{\eta})$ quantifies the amount of information available in the received signal in (6) about these parameters and it is computed as

$$\mathbf{J}_{\boldsymbol{\eta}} = \begin{bmatrix} \mathbf{J}_{\boldsymbol{\theta}_{\mathrm{RX}}\boldsymbol{\theta}_{\mathrm{RX}}} & \mathbf{J}_{\boldsymbol{\theta}_{\mathrm{RX}}\boldsymbol{\theta}_{\mathrm{TX}}} & \cdots & \mathbf{J}_{\boldsymbol{\theta}_{\mathrm{RX}}\boldsymbol{\tau}} \\ \mathbf{J}^{\mathrm{T}}_{\boldsymbol{\theta}_{\mathrm{RX}}\boldsymbol{\theta}_{\mathrm{TX}}} & \mathbf{J}_{\boldsymbol{\theta}_{\mathrm{TX}}\boldsymbol{\theta}_{\mathrm{TX}}} & \cdots & \mathbf{J}_{\boldsymbol{\theta}_{\mathrm{TX}}\boldsymbol{\tau}} \\ \vdots & \cdots & \ddots & \vdots \\ \mathbf{J}^{\mathrm{T}}_{\boldsymbol{\theta}_{\mathrm{RX}}\boldsymbol{\tau}} & \mathbf{J}^{\mathrm{T}}_{\boldsymbol{\theta}_{\mathrm{TX}}\boldsymbol{\tau}} & \cdots & \mathbf{J}_{\boldsymbol{\tau}\boldsymbol{\tau}} \end{bmatrix}, \tag{8}$$

where each entry of the FIM is defined as

$$[\mathbf{J}_{\boldsymbol{\eta}}]_{u,v} \triangleq \frac{1}{N_0} \int_0^{N_s T_s} \mathbb{E}_{\mathrm{d}} \left[\Re \left\{ \frac{\partial \boldsymbol{\mu}(t)^{\mathrm{H}}}{\partial [\boldsymbol{\eta}]_u} \frac{\partial \boldsymbol{\mu}(t)}{\partial [\boldsymbol{\eta}]_v} \right\} \right] dt, \tag{9}$$

with $\mathbb{E}_{\mathrm{d}}[\cdot]$ denotes the expectation with respect to the pilot symbols, $\Re(\cdot)$ is the real part of the argument. The FIM is related to the estimation error covariance matrix of any unbiased estimator via the information inequality

$$\mathbb{E}\left[(\boldsymbol{\eta} - \hat{\boldsymbol{\eta}})(\boldsymbol{\eta} - \hat{\boldsymbol{\eta}})^{\mathrm{T}}\right] \succeq \mathbf{J}_{\boldsymbol{\eta}}^{-1}, \tag{10}$$

where $\hat{\boldsymbol{\eta}}$ refers to the estimate of $\boldsymbol{\eta}$ and $\mathbf{A} \succeq \mathbf{B}$ is equivalent to $\mathbf{A} - \mathbf{B}$ being positive semi-definite. The inequality in (10) is the CRLB. The FIM can be rearranged via a permutation of its entries as

$$\mathbf{J}_{\tilde{\boldsymbol{\eta}}} = \mathrm{blkdiag}(\mathbf{J}_{\boldsymbol{\eta},1}, \ldots, \mathbf{J}_{\boldsymbol{\eta},K}), \tag{11}$$

where the reordered matrix $\mathbf{J}_{\tilde{\boldsymbol{\eta}}}$ groups together the parameters associated with the same propagation path. This block-diagonal structure highlights the individual contribution of each kth path to the overall CRLB. In order to map the CRLB computed for $\boldsymbol{\eta}$ to the PEB, we convert the FIM over channel parameters to one expressed in terms of TX position $\mathbf{p}$ as

$$\mathbf{J}_{\boldsymbol{p}} = \mathbf{T} \mathbf{J}_{\tilde{\boldsymbol{\eta}}} \mathbf{T}^{\mathrm{T}}, \tag{12}$$

where $\mathbf{T}$ is transformation matrix defined

$$\mathbf{T} \triangleq \left[\begin{array}{c|ccc} \mathbf{T_p}^{(1)} & \mathbf{T_p}^{(2)} & \cdots & \mathbf{T_p}^{(K)} \\ \hline 0 & \mathbf{T_s}^{(2)} & \cdots & 0 \\ \vdots & \vdots & \ddots & \vdots \\ 0 & 0 & \cdots & \mathbf{T_s}^{(K)} \end{array}\right] \triangleq \left[\begin{array}{c|c} \mathbf{A} & \mathbf{B} \\ \hline \mathbf{0} & \mathbf{D} \end{array}\right], \tag{13}$$

with $\mathbf{T_p}^{(k)} \in \mathbb{R}^{3 \times 5}$

$$\mathbf{T_p}^{(k)} = \begin{bmatrix} \frac{\partial \theta_{\mathrm{RX},k}}{\partial \mathbf{p}} & \frac{\partial \theta_{\mathrm{TX},k}}{\partial \mathbf{p}} & \frac{\partial \phi_{\mathrm{RX},k}}{\partial \mathbf{p}} & \frac{\partial \phi_{\mathrm{TX},k}}{\partial \mathbf{p}} & \frac{\partial \tau_k}{\partial \mathbf{p}} \end{bmatrix}, \tag{14}$$

and $\mathbf{T}_s^{(k)} \in \mathbb{R}^{3 \times 5}$

$$\mathbf{T_s}^{(k)} = \begin{bmatrix} \frac{\partial \theta_{\mathrm{RX},k}}{\partial \mathbf{s_k}} & \frac{\partial \theta_{\mathrm{TX},k}}{\partial \mathbf{s_k}} & \frac{\partial \phi_{\mathrm{RX},k}}{\partial \mathbf{s_k}} & \frac{\partial \phi_{\mathrm{TX},k}}{\partial \mathbf{s_k}} & \frac{\partial \tau_k}{\partial \mathbf{s_k}} \end{bmatrix}. \tag{15}$$

By solving the matrix product in (13) the FIM can be written as

$$\mathbf{J_p} = \begin{bmatrix} \mathbf{A}\mathbf{J}_{\boldsymbol{\eta}_{\mathrm{LOS}}}\mathbf{A}^{\mathrm{T}} + \mathbf{B}\mathbf{J}_{\boldsymbol{\eta}_{\mathrm{NLOS}}}\mathbf{B}^{\mathrm{T}} & \mathbf{B}\mathbf{J}_{\boldsymbol{\eta}_{\mathrm{NLOS}}}\mathbf{D}^{\mathrm{T}} \\ \mathbf{D}\mathbf{J}_{\boldsymbol{\eta}_{\mathrm{NLOS}}}\mathbf{B}^{\mathrm{T}} & \mathbf{D}\mathbf{J}_{\boldsymbol{\eta}_{\mathrm{NLOS}}}\mathbf{D}^{\mathrm{T}} \end{bmatrix}, \tag{16}$$

where $\mathbf{J}_{\boldsymbol{\eta}_{\mathrm{LOS}}} = \mathbf{J}_{\boldsymbol{\eta},1}$ refers to the LOS path, while $\mathbf{J}_{\boldsymbol{\eta}_{\mathrm{NLOS}}} = \mathrm{blkdiag}(\mathbf{J}_{\boldsymbol{\eta},2}, \ldots, \mathbf{J}_{\boldsymbol{\eta},K})$ is related to the NLOS paths. In order to isolate and quantify the localization information loss or gain associated with LOS and NLOS contributions, the Schur complement is applied to the FIM to obtain the Equivalent Fisher Information Matrix (EFIM)

$$\begin{aligned} \mathbf{J}^e_{\mathbf{p}} = & \underbrace{\mathbf{A}\mathbf{J}_{\boldsymbol{\eta}_{\mathrm{LOS}}}\mathbf{A}^{\mathrm{T}}}_{\text{LOS gain}} + \underbrace{\mathbf{B}\mathbf{J}_{\boldsymbol{\eta}_{\mathrm{NLOS}}}\mathbf{B}^{\mathrm{T}}}_{\text{NLOS gain}} \\ & - \underbrace{\mathbf{B}\mathbf{J}_{\boldsymbol{\eta}_{\mathrm{NLOS}}}\mathbf{D}^{\mathrm{T}}(\mathbf{D}\mathbf{J}_{\boldsymbol{\eta}_{\mathrm{NLOS}}}\mathbf{D}^{\mathrm{T}})^{-1}\mathbf{D}\mathbf{J}_{\boldsymbol{\eta}_{\mathrm{NLOS}}}\mathbf{B}^{\mathrm{T}}}_{\text{NLOS loss}}. \end{aligned} \tag{17}$$

Notably, the EFIM can be decomposed into three distinct components that explicitly capture the contributions of (i) the LOS gain, (ii) the NLOS gain, and (iii) the NLOS loss. The latter term reflects the fact that the inclusion of NLOS components may not always be beneficial: while some NLOS paths enhance the localization accuracy, others may

[1] For analytical tractability in urban environments, NLOS propagation is modeled as consisting of single-bounce reflections.

[2] We adopt a narrowband array model and assume the channel is quasi-time-invariant over a symbol interval. This is justified even for sub-6 GHz systems in typical urban settings with moderate vehicular speeds (< 50 km/h), where Doppler shifts (< 80 Hz) cause only minor phase rotations, negligible compared to the dominant spatial and multipath effects.

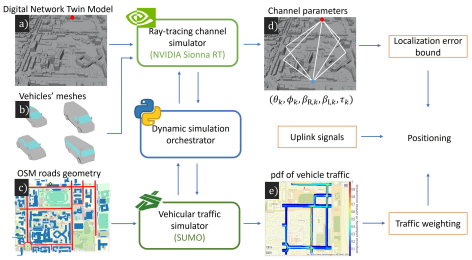

Fig. 2: The proposed framework integrates static geometry and dynamic traffic data into SUMO and a Python orchestrator, feeding the Sionna-RT ray tracer to generate time-varying channel parameters used, along with uplink signals and traffic weights, to compute localization error bounds.

degrade it due to increased uncertainty or geometric dilution. Consequently, only those NLOS paths for which the difference between their gain and loss contributions is strictly positive effectively contribute to improving the overall localization performance.

Finally, the PEB, which characterizes the lower bound on the root mean square error of the unbiased estimator of the position vector $\mathbf{p}$, is given by

$$\text{PEB} = \sqrt{\text{tr}\{(\mathbf{J}_{\mathbf{p}}^{e})^{-1}\}}. \tag{18}$$

The computation of the FIM and the corresponding CRLB, including the PEB, relies on accurate knowledge of multipath channel parameters. In urban wireless environments, such estimation is particularly challenging due to the presence of dynamic propagation conditions and complex multipath interactions. By leveraging NDT, however, it becomes feasible to extract these parameters with high precision through traffic-aware modeling and high-fidelity ray-tracing simulations.

IV. 3D Localization Leveraging NDT

This section introduces the proposed NDT framework and demonstrates how it facilitates improved localization accuracy through the design of an optimal precoder.

A. NDT Framework

As illustrated in Fig. 2, the NDT is a simulation framework designed to replicate real-world urban environments for the analysis and optimization of wireless systems. It combines detailed geographic data (Figs. 2 a and b), realistic vehicle mobility (Fig. 2c), and accurate electromagnetic propagation models (Fig. 2d) to provide a dynamic and high-fidelity representation of network scenarios. A dynamic orchestrator integrates these parameters with realistic mobility and road topology information sourced from OpenStreetMap (OSM). Vehicular dynamics and trajectories are simulated using Simulation of Urban Mobility (SUMO) software. Figure 2(e) illustrates the empirical probability of vehicle occurrence across the considered area, highlighting regions with varying traffic densities. It can be observed that vehicle density is significantly higher at intersections and main roads, where traffic flow is more concentrated.

The output of the NDT consists of communication channel parameters computed at each time step and for each spatial grid cell, where the area of interest is discretized into elementary units of 2m $\times$ 2m. For each grid cell, the NDT provides per-path channel characteristics, including angles of arrival/departure (θ_k, ϕ_k), complex path gains $(\beta_{R,k}, \beta_{I,k})$, and delays (τ_k). [3]

The channel information extracted from the NDT framework is incorporated into the uplink signal processing to evaluate localization performance metrics, namely the CRLB and the PEB. These metrics guide a precoding strategy that prioritizes propagation paths beneficial to localization. Additionally, spatial traffic distributions enable a traffic-aware weighting scheme that further refines the precoder. The detailed formulation is presented in the next subsection.

B. NDT-based Precoder Optimization

Leveraging the NDT framework, we propose a precoder optimization strategy aimed at improving localization accuracy. Conventional approaches often employ a large number of beams (N_B) to uniformly probe the angular domain, leading to redundant spatial transmissions [13]. However, analysis of PEB derived from NDT data reveals that only a small subset of multipath components significantly contributes to localization.

We quantify the benefit of incorporating NLOS paths via:

$$\Delta_{\text{PEB}} = \frac{\text{PEB}_{\text{LOS}} - \text{PEB}_{\text{LOS+NLOS}}}{\text{PEB}_{\text{LOS}}} \times 100\%, \tag{19}$$

where PEB_{LOS} is computed using only the LOS path, and $\text{PEB}_{\text{LOS+NLOS}}$ includes both LOS and NLOS components. Results show that among the $K-1$ NLOS paths, a single dominant reflector often provides most of the PEB gain.

Based on this insight, we define an optimized precoder:

$$\mathbf{F}_{\text{opt}} = \left[\boldsymbol{f}_{\text{LOS}} \quad \boldsymbol{f}_{\mathbf{s}_k^*}\right], \tag{20}$$

where $\mathbf{f}_{\text{LOS}}$ targets the LOS path and $\mathbf{f}_{\mathbf{s}_k^*}$ steers toward the most effective NLOS path.

A key challenge is that the optimal NLOS direction depends on the user position, which is itself unknown. To address this, we assume access to a coarse initial position estimate (e.g., from initial access or historical data), which limits the search space to a region where only a subset of reflectors is relevant. Importantly, there is no strict one-to-one correspondence between user position and optimal reflector: a single dominant NLOS path typically benefits a cluster of nearby locations, as shown in Fig.3. This enables the system to robustly select a beam pair even under localization uncertainty.

In practice, $\mathbf{f}_{\text{LOS}}$ can be estimated during initial access and synchronization, while $\mathbf{f}_{\mathbf{s}_k^*}$ is selected based on its expected contribution to PEB reduction within the cluster of candidate positions. The corresponding azimuth and elevation angles are then quantized to the nearest entry in the beam-steering

[3]Doppler effects are not explicitly modeled at the per-symbol basis in the NDT; instead, the channel is evaluated under a quasi-static snapshot assumption, where each time instance represents a channel realization within a duration shorter than the coherence time.

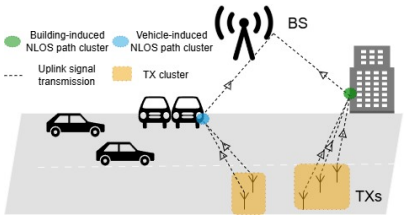

Fig. 3: Cluster-based dominant-NLOS selection. TXs are grouped into spatial clusters of about five TXs, with an average cluster radius of 6.4 m computed from NDT statistics.

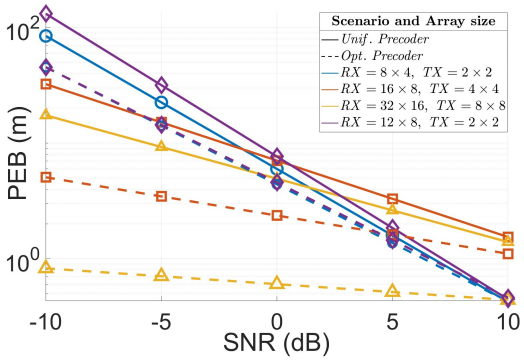

Fig. 4: PEB vs. SNR with LOS and dominant NLOS path, comparing uniform and optimized precoders across diverse antenna configurations.

codebook to synthesize the final precoder. Moreover, the NDT's dynamic channel representation allows periodic updates of this strategy, enabling real-time adaptation to mobility and ensuring consistent localization accuracy over time as explained in the next subsection.

C. Joint NDT- and Traffic-Aware Precoder Optimization

While the NDT framework enables high-fidelity modeling of urban wireless environments, real-time updates are often infeasible due to the inherently dynamic nature of vehicular traffic. To address this limitation, we propose a probabilistic precoding strategy that incorporates long-term vehicle occurrence statistics into the optimization process.

The NDT discretizes the simulation area into spatial bins of size $2\,\mathrm{m} \times 2\,\mathrm{m}$. For each bin b, we define the probability $P_r[b]$ that a reflector r is present within it:

$$P_r[b] = \begin{cases} 1, & \text{if } r \text{ is static (e.g., building, tree)} \\ \frac{T_r}{T_{\text{tot}}}, & \text{if } r \text{ is a vehicle} \end{cases} \tag{21}$$

where T_r is the number of time steps in which the vehicle r is detected as a reflector in bin b, and T_{tot} is the total number of time steps in the NDT simulation. This probabilistic model captures the spatial-temporal distribution of mobile reflectors such as cars or buses as shown in Fig. 2e.

Reflectors induce NLOS paths, each contributing differently to localization accuracy. These contributions are captured by the path-specific FIM $\mathbf{J}_k$ for the k-th NLOS path (with $k \geq 2$). We define a probability-weighted FIM that incorporates the likelihood of each path's availability:

$$\mathbf{J}_{\text{weighted}} = \sum_{k \geq 2} P_r(\mathbf{s}_k) \cdot \mathbf{J}_k, \tag{22}$$

where $P_r(\mathbf{s}_k)$ denotes the probability of the k-th path being active, based on the spatial presence of its associated reflector at position $\mathbf{s}_k$. The probability $P_r(\mathbf{s}_k)$ is derived from the spatial reflector distribution in (21), where $\mathbf{s}_k$ lies within bin b associated with reflector r. That is, $P_r(\mathbf{s}_k) = P_r[b]$ if path k is induced by reflector r located in bin b.

This formulation recognizes that not all NLOS paths are equally likely or beneficial. By weighting the FIM according to reflector availability, it emphasizes paths that are both geometrically informative and statistically probable. After computing the probabilistic EFIM, the PEB is recomputed using (18) and (19). The optimized precoder, derived as in (20), robustly adapts to traffic uncertainty by balancing instantaneous geometric information with long-term traffic dynamics.

V. Numerical Results

We model a realistic urban scenario using the Politecnico di Milano High-Frequency campus and a 2.5D map within the NDT simulation, integrating dynamic SUMO-generated vehicular traces with Sionna-based ray tracing [4], where vehicle positions influence propagation. The TX is randomly placed, while the BS is fixed at $\mathbf{b} = [-80.5, 245.5, 21.7]^{\mathrm{T}}$. Both TX and RX use UPAs with half-wavelength spacing at a carrier frequency of $f_c = 7$GHz. A 100MHz sinc pilot with $E_s/T_s = 0$ dBm, $N_0 = -160$ dBm/Hz, and $N_s = 16$ symbols is transmitted. Under uniform beamforming, $N_B = 50$ beams span azimuth and elevation. User location uncertainty is modeled as a 4-meter standard deviation Gaussian prior, guiding dominant NLOS path selection within a spatial cluster.

Figure 4 shows the PEB versus signal-to-noise (SNR) for the proposed optimized precoder and the conventional uniform codebook-based precoder [13], using NDT data across various array configurations. On average, the proposed precoder yields a $2\times$ gain at high SNR (≥ 5 dB) and up to $10\times$ at low SNR. For example, the average PEB drops from 80 m to 10 m at low SNR, and from 1.2 m to 0.6 m at high SNR when exploiting the proposed optimized precoder. Performance improves with array size, particularly with more TX elements, due to increased beamforming gain. The optimized precoder consistently outperforms the uniform one by adaptively steering energy toward LOS and dominant NLOS paths, enhancing robustness in urban localization scenarios.

The impact of vehicle-induced NLOS paths is illustrated in Fig. 5, which presents the cumulative density function (CDF) of the PEB for the proposed optimized precoder and the uniform precoder. Both precoders are evaluated in two configurations: non-weighted and weighted according to vehicular traffic statistics. The TX is positioned on top of the vehicle roof, with an antenna array of size $N_{\text{TX}} = 2\times2$, while the RX is equipped with an antenna array of $N_{\text{RX}} = 12 \times 8$

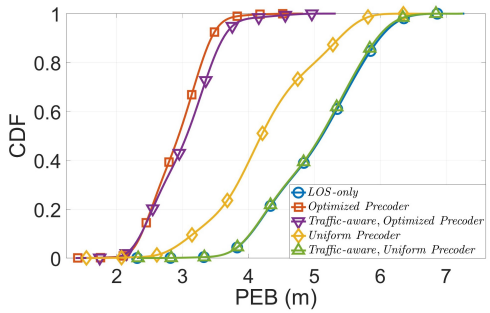

Fig. 5: CDF of uplink PEB with vehicle-induced reflectors under deterministic and traffic-weighted modeling.

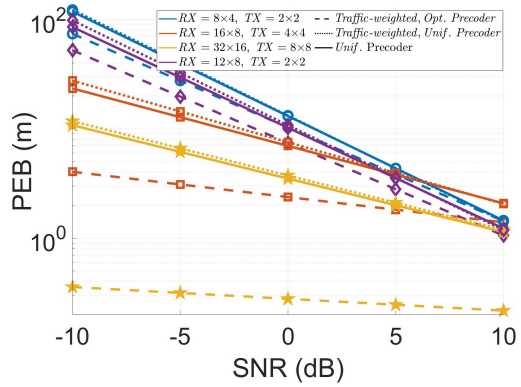

Fig. 6: PEB vs. SNR using traffic-weighted NLOS paths under various antenna configurations.

elements. The optimized precoder, informed by NDT, reduces the mean PEB by nearly 35% both with and without traffic weighting, highlighting the effectiveness of integrating traffic statistics with path-aware precoding. Introducing vehicular traffic statistics does not significantly degrade the performance of the optimized precoder while providing a more robust solution across temporal and spatial variations. In contrast, the uniform precoder results in a higher average PEB, as it fails to adapt to traffic variations, making it more susceptible to traffic distribution. Additionally, leveraging effective NLOS paths improves localization performance, reducing the average PEB by a factor of 2 with the optimized precoder compared to when only the LOS path is considered.

To further validate the approach, Fig. 6 reports PEB across SNR and antenna configurations using traffic-weighted NLOS paths only. The traffic-aware optimized precoder consistently outperforms the uniform precoder , demonstrating the benefit of leveraging site-specific NDT. Unlike conventional approaches that rely on static datasets, NDT captures recurring vehicular mobility patterns through spatiotemporal traffic priors, improving localization robustness in dynamic V2X settings.

VI. Conclusion

In this paper, we derived a theoretical bound on localization error within an NDT-enabled communication framework by utilizing a priori vehicular traffic data and precise channel parameters. Our proposed method dynamically computes the Position Error Bound in a manner that closely mirrors real-world conditions. It also demonstrates the potential of vehicles to function as effective reflectors for localization tasks in urban environments. Simulation results show that using an NDT-empowered optimized precoder for vehicle reflectors can yield approximately a 35% improvement in localization performance over uniform precoder, highlighting the advantages of a robust NDT framework and suggesting that modeling traffic probability distributions can further refine precoder design. Overall, this work emphasizes the efficacy of NDT approaches in urban V2X and CAV scenarios, laying the groundwork for more robust and dynamic localization solutions.

References

[1] M. Noor-A-Rahim, Z. Liu, H. Lee, M. O. Khyam, J. He, D. Pesch, K. Moessner, W. Saad, and H. V. Poor, "6g for vehicle-to-everything (v2x) communications: Enabling technologies, challenges, and opportunities," *Proceedings of the IEEE*, vol. 110, no. 6, pp. 712–734, 2022.

[2] L. U. Khan, W. Saad, D. Niyato, Z. Han, and C. S. Hong, "Digital-twin-enabled 6g: Vision, architectural trends, and future directions," *IEEE Communications Magazine*, vol. 60, no. 1, pp. 74–80, 2022.

[3] L. Cazzella, F. Linsalata, M. Magarini, M. Matteucci, and U. Spagnolini, "A multi-modal simulation framework to enable digital twin-based v2x communications in dynamic environments," *ArXiv*, vol. abs/2303.06947, 2023. [Online]. Available: https://api.semanticscholar.org/CorpusID:257496641

[4] R. Pegurri, F. Linsalata, E. Moro, J. Hoydis, and U. Spagnolini, "Toward digital network twins: Integrating sionna RT in ns-3 for 6G Multi-RAT networks simulations," in *IEEE INFOCOM WKSHPS: Digital Twins over NextG Wireless Networks (DTWIN 2025) (INFOCOM DTWIN 2025)*, London, United Kingdom (Great Britain), May 2025, p. 5.88.

[5] A. Alkhateeb, S. Jiang, and G. Charan, "Real-time digital twins: Vision and research directions for 6g and beyond," *IEEE Communications Magazine*, vol. 61, no. 11, pp. 128–134, 2023.

[6] A. Shahmansoori, G. E. Garcia, G. Destino, G. Seco-Granados, and H. Wymeersch, "Position and orientation estimation through millimeter-wave mimo in 5g systems," *IEEE Transactions on Wireless Communications*, vol. 17, no. 3, pp. 1822–1835, 2018.

[7] Z. Cui, P. Zhang, and S. Pollin, "6g wireless communications in 7-24 ghz band: Opportunities, techniques, and challenges," 2024. [Online]. Available: https://arxiv.org/abs/2310.06425

[8] J. Morais and A. Alkhateeb, "Localization in digital twin mimo networks: A case for massive fingerprinting," in *2024 IEEE International Conference on Communications Workshops (ICC Workshops)*, 2024, pp. 276–281.

[9] F. Linsalata, S. Mura, M. Mizmizi, M. Magarini, P. Wang, M. N. Khormuji, A. Perotti, and U. Spagnolini, "Los-map construction for proactive relay of opportunity selection in 6g v2x systems," *IEEE Transactions on Vehicular Technology*, vol. 72, no. 3, pp. 3864–3878, 2023.

[10] J. Li, M. F. Da Costa, and U. Mitra, "Joint localization and orientation estimation in millimeter-wave mimo ofdm systems via atomic norm minimization," *IEEE Transactions on Signal Processing*, vol. 70, pp. 4252–4264, 2022.

[11] R. Mendrzik, H. Wymeersch, G. Bauch, and Z. Abu-Shaban, "Harnessing nlos components for position and orientation estimation in 5g millimeter wave mimo," *IEEE Transactions on Wireless Communications*, vol. 18, no. 1, pp. 93–107, 2019.

[12] X. Chu, Z. Lu, D. Gesbert, L. Wang, and X. Wen, "Vehicle localization via cooperative channel mapping," *IEEE Transactions on Vehicular Technology*, vol. 70, no. 6, pp. 5719–5733, 2021.

[13] M. Giordani, M. Mezzavilla, and M. Zorzi, "Initial access in 5g mmwave cellular networks," *IEEE Communications Magazine*, vol. 54, no. 11, pp. 40–47, 2016.